



**Scholars Research Library**

Archives of Applied Science Research, 2010, 2 (5):199-208

(<http://scholarsresearchlibrary.com/archive.html>)



ISSN 0975-508X

CODEN (USA) AASRC9

## **Studies on the structural, optical and mechanical properties of non-linear optical single crystal: 4-Methoxy benzaldehyde -N-methyl 4-stilbazolium tosylate**

**Amirdha Sher Gill<sup>1</sup>, S. Kalainathan<sup>1\*</sup> and G. Bhagavannarayana<sup>2</sup>**

<sup>1</sup>*School of Advanced Sciences, VIT University, Vellore, Tamil Nadu, India*

<sup>2</sup>*CGC Division, National Physical Laboratory, New Delhi, India*

---

### **ABSTRACT**

*Organic non-linear optical single crystal 4-methoxy benzaldehyde - N -methyl - 4 - stilbazolium tosylate (MBST) has been synthesised and grown by slow evaporation technique. The grown crystals were analyzed by various instrumentation techniques. The crystal system and lattice parameters were found from single crystal X-ray diffraction. The crystalline perfection is quite good as observed from the high resolution X-ray diffractometry. The FTIR spectrum gives the detail about the various functional groups present and the UV-vis-NIR studies show that the crystal is optically transparent in the wavelength range of 440–1100 nm. The powder SHG studies were done with Kurtz powder technique and the NLO efficiency is 17.2 times greater than urea. Mechanical behavior was analyzed using Vicker's microhardness test. Microhardness studies revealed that the hardness of the grown crystal increases with an increase in load. Meyer's index number n was calculated and found that the material belongs to soft material category.*

**Keywords:** organic compounds, crystal growth, High resolution X-ray diffraction, crystal structure, mechanical properties.

---

### **INTRODUCTION**

The design of nonlinear optical (NLO) molecules has become a focus of current research in view of their potential applications in various photonic technologies. NLO is one of the few modern scientific frontiers where the interest is not only for understanding of new physical phenomena, but also to realize the technological applications. The NLO process requires materials that

199

manipulate the amplitude, phase, polarization and frequency of optical beams. While variety of materials including inorganic, organic and polymeric have been studied for their NLO activity, it is the organic materials which have been receiving the maximum attention [1-4]. Much effort has been spent in the design of new molecules with high molecular nonlinearities that would promote a better noncentrosymmetric crystal packing and enable an easier bulk growth of crystals with various degrees of success [5]. One of the stilbazolium derivatives is 4-Methoxy benzaldehyde N-methyl 4-stilbazolium tosylate (MBST), which has been demonstrated to exhibit large second harmonic generation, 17 times greater than urea [6]. Though MBST has been reported synthesized, we present here in this article FTIR, UV, HRXRD spectral analysis, and dielectric measurements of MBST. However, to the best of our knowledge there is no report of the titled material on the study of crystalline perfection, morphology, and mechanical studies are available. In the present investigation, the single crystals of MBST were grown successfully by slow cooling technique. The crystal structure was confirmed by X-ray diffraction. The crystalline perfection was assessed by high-resolution X-ray diffractometry (HRXRD). SHG, optical transmission, chemical etching and microhardness studies were also carried out.

## MATERIALS AND METHODS

### 2.1. Synthesis and growth

The title compound was synthesized by the condensation reaction of 4-methyl-N-methyl pyridinium tosylate, which was prepared from 4-picoline, methyl p-toluene sulfonate and 4-methoxy benzaldehyde in the presence of piperidine. The calculated amounts of picoline and methyl toluene sulphonate were added to toluene solution taken in a round bottom flask of Dean and Stark apparatus. The mixture was heated in the heating mantle until it crystallizes as white salt insoluble in toluene. Dimethyl formamide was added in plenty to dissolve the white salt until the solution becomes very clear and 4-methoxy benzaldehyde was added to the clear solution. Few drops of piperidine were added and the color of the solution turns green. Then the mixture was refluxed in a Dean-Stark trap in order to remove water. After the collection of more than an equivalent amount of water the reactants were cooled to room temperature and yellow color MBST salt was collected. The collected material was kept in the oven at 120 °C for an hour to get rid of the absorption of water from the atmosphere. The synthesized material was dissolved in methanol, and was transferred to a heavy walled tray with fine pored cover and was left undisturbed. Purification was effected by recrystallizing at least three times from methanol. Transparent crystals of size 12 mm x 4 mm x 3 mm were harvested after six such successive recrystallisation processes (Fig. 1).



Fig. 1. Photograph of the grown crystal

## 2.2 Characterization

The single crystal X-ray diffraction intensity data were collected at 233K (-40°C) on a Stoe Mark II-Image Plate Diffraction System [7] equipped with a two-circle goniometer and using MoK $\alpha$  graphite monochromated radiation ( $\lambda = 0.71073 \text{ \AA}$ ). Image plate distance 130 mm,  $\omega$  rotation scans 0 - 180° at  $\phi$  0°, and 0 – 180.0° at  $\phi$  90°, step  $\Delta\omega = 1.5^\circ$ , exposures of 3 min per image, 2 $\theta$  range 1.76 - 52.59°,  $d_{\min} - d_{\max} = 23.107 - 0.802 \text{ \AA}$ .

The structure was solved by direct methods [8] and the R-values of the full-matrix least squares refinements [8] are given in Table 1. All atoms except hydrogen atoms and atoms of disordered molecules were refined anisotropically. H-atoms were placed at calculated positions on the basis of stereo-chemical considerations and refined according to the riding model.

CCDC 774844 contains the supplementary crystallographic data for MBST and this data can be obtained free of charge from The Cambridge Crystallographic Data Centre([www.ccdc.cam.ac.uk/data\\_request/cif](http://www.ccdc.cam.ac.uk/data_request/cif)).

**Table 1. Crystal Data**

Crystal System	Triclinic		
Space group	P1 (No. 1)		
a, b, c [ $\text{\AA}$ ]	6.7387(11)	7.8877(13)	9.6118(15)
$\alpha, \beta, \gamma$ [°]	79.002(12)	80.617(13)	83.823(13)
V [ $\text{\AA}^3$ ]		493.26(14)	
Z		1	
D(calc) [g/cm <sup>3</sup> ]		1.338	

The crystalline perfection of the grown single crystals was characterized by HRXRD by employing a multicrystal X-ray diffractometer developed at NPL [9]. The well-collimated and monochromated MoK $\alpha_1$  beam obtained from the three monochromator Si crystals set in dispersive (+,-,-) configuration has been used as the exploring X-ray beam. The specimen crystal is aligned in the (+,-,-,+ ) configuration. Due to dispersive configuration, though the lattice constant of the monochromator crystal(s) and the specimen are different, the unwanted dispersion broadening in the diffraction curve (DC) of the specimen crystal is insignificant. The specimen can be rotated about the vertical axis, which is perpendicular to the plane of diffraction, with minimum angular interval of 0.4 arc s. The rocking or diffraction curves were recorded by changing the glancing angle (angle between the incident X-ray beam and the surface of the specimen) around the Bragg diffraction peak position  $\theta_B$  (taken as zero for the sake of convenience) starting from a suitable arbitrary glancing angle and ending at a glancing angle after the peak so that all the meaningful scattered intensities on both sides of the peak include in the diffraction curve. The DC was recorded by the so-called  $\omega$  scan wherein the detector was kept at the same angular position 2 $\theta_B$  with wide opening for its slit. This arrangement is very appropriate to record the short range order scattering caused by the defects or by the scattering from local Bragg diffractions from agglomerated point defects or due to low angle and very low angle structural grain boundaries [10]. Before recording the diffraction curve to remove the non-crystallized solute atoms remained on the surface of the crystal and the possible layers which

may sometimes form on the surfaces on crystals grown by solution methods [11] and also to ensure the surface planarity, the specimen was first lapped and chemically etched in a non preferential etchant of water and acetone mixture in 1:2 volume ratio.

The FTIR spectra was recorded using AVATAR -330 FTIR thermo nicolet spectrophotometer in the wavelength range 400-4000 cm<sup>-1</sup> by KBr pellet technique. UV-Vis spectrum was recorded in solution state by a Hitachi U2800 double beam spectrometer with a band pass of 1.5 nm. Mitutoyo MH 112, Japan was employed for Microhardness testing measurements at room temperature.

## RESULTS AND DISCUSSION

### 3.1 Single crystal X-ray diffraction

The calculated lattice parameters shows that that the MBST crystal belongs to triclinic system with space group P1, and the observed lattice parameters are  $a = 6.7540 (5)$  Å,  $b = 7.9067 (5)$  Å,  $c = 9.6181 (6)$  Å,  $\alpha = 78.905 (3)^\circ$ ,  $\beta = 80.589 (3)^\circ$ ,  $\gamma = 83.580 (3)^\circ$  and Volume  $V = 513.624 (5)$  Å<sup>3</sup>. The observed values are in good agreement with the reported literature values [6]. The molecular structure and crystallographic numbering scheme are illustrated in Fig. 2, displacement ellipsoids are drawn at the 50% probability level. Perspective view along the  $a$ -axis of the crystal packing, with C-H...O interactions shown as dashed lines, is shown in Fig. 3.

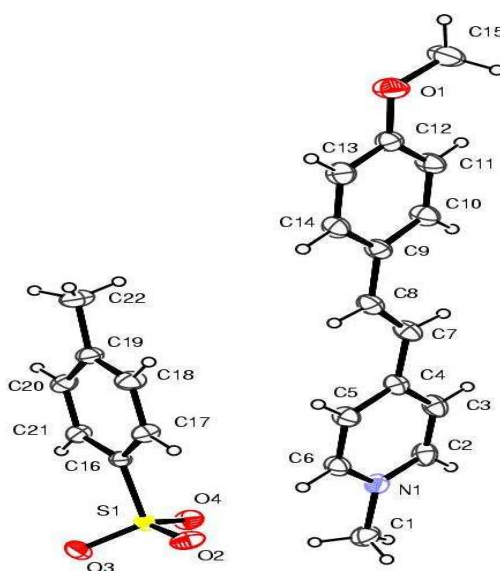


**Fig. 2. The molecular structure with numbering scheme**

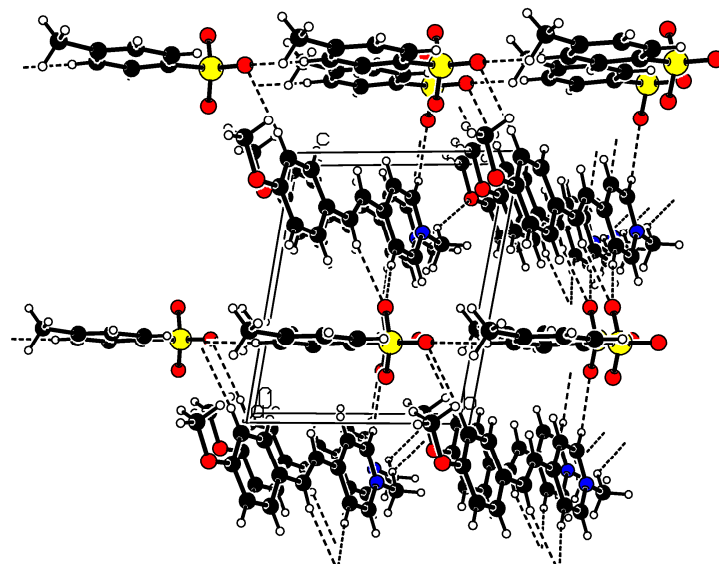
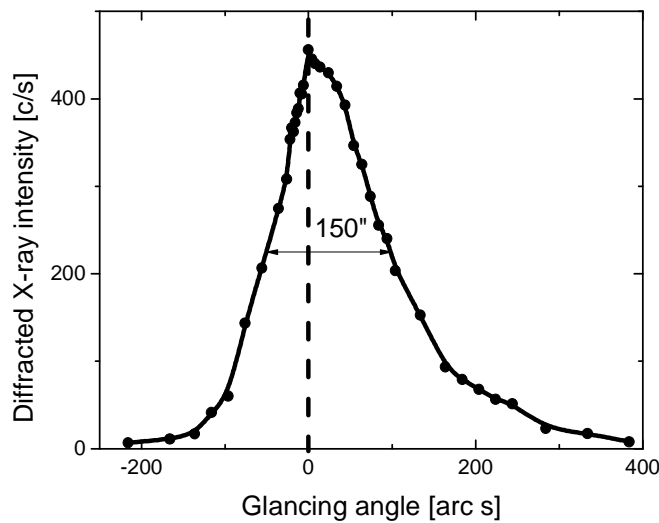


**Fig. 3 Crystal packing viewed along  $a$ -axis.**

### 3.2 High resolution X-ray diffraction Analysis

Fig. 4 shows the high-resolution diffraction curve (DC) recorded for a typical MBST single crystal using (0-10) diffracting planes in symmetrical Bragg geometry by employing the multicrystal X-ray diffractometer with MoK $\alpha_1$  radiation. As seen in the figure, the DC contains a single peak and indicates that the specimen is free from structural grain boundaries. The FWHM (full width at half maximum) of the curve is 150 arc s which is somewhat more than that expected for an ideally perfect crystal from the plane wave theory of dynamical X-ray diffraction [12], but close to that expected for a nearly perfect real life crystal. It is interesting to see the asymmetry of the DC. For a particular angular deviation ( $\Delta\theta$ ) of glancing angle with respect to the peak position, the scattered intensity is much more in the positive direction in comparison to that of the negative direction. This feature clearly indicates that the crystal contains predominantly interstitial type of defects than that of vacancy defects. This can be well understood by the fact that due to interstitial defects (self interstitials or impurities at interstitial sites), which may be due to fast growth and/or impurities present in the raw material, the lattice around these defects undergo compressive stress [13] and the lattice parameter  $d$  (interplanar spacing) decreases and leads to give more scattered (also known as diffuse X-ray scattering) intensity at slightly higher Bragg angles ( $\theta_B$ ) as  $d$  and  $\sin \theta_B$  are inversely proportional to each other in the Bragg equation ( $2d \sin \theta_B = n\lambda$ ;  $n$  and  $\lambda$  being the order of reflection and wavelength respectively which are fixed). However, the single diffraction curve with reasonably low FWHM indicates that the crystalline perfection is fairly good. The density of such interstitial defects is however very meager and in almost all real crystals including nature gifted crystals, such defects are commonly observed and are many times unavoidable due to thermodynamical conditions and hardly affect the device performance. More details may be obtained from the study of high-resolution diffuse X-ray scattering measurements [14], which is however not the main focus of the present investigation. It is worth to mention here that the observed scattering due to interstitial defects is of short order nature as the strain due to such minute defects is limited to the very defect core and the long order could not be expected and hence the change in the lattice parameter of the

crystal is not possible. It may be mentioned here that the minute information like the asymmetry in the DC could be possible as in the present sample only because of the high-resolution of the multicrystal X-ray diffractometer used in the present investigation. Fig. 4 Diffraction curve of MBST crystal for 010 plane



### 3.3 Fourier Transform Infrared Spectroscopic Studies

The FTIR spectrum was recorded using Avatar 330 FT-IR thermonicolet spectrometer in the wavelength range 400–4000 cm<sup>-1</sup> by KBr pellet technique. The middle infrared (IR) spectrum of the MBST material is shown in Fig. 5 and the functional groups were identified and tabulated (Table 2).

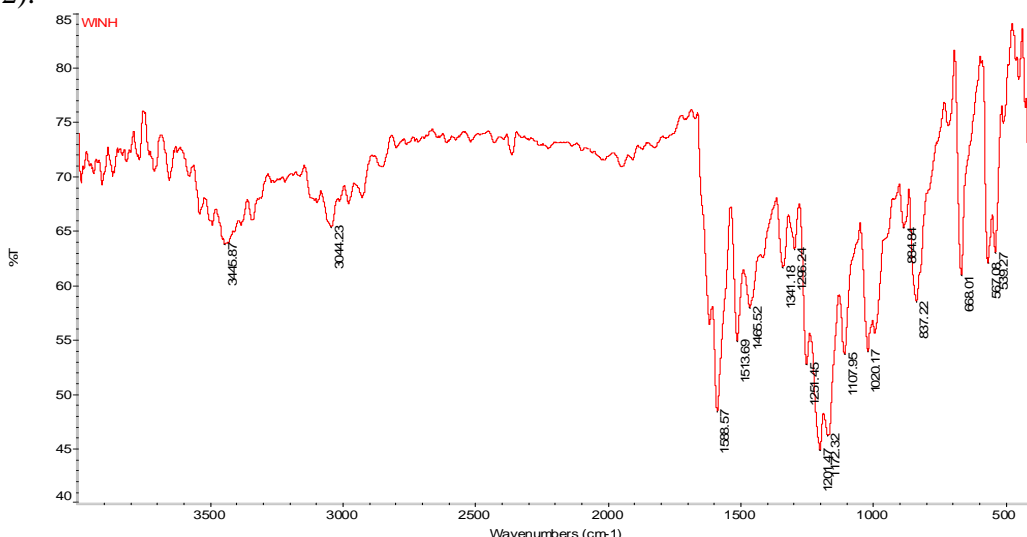


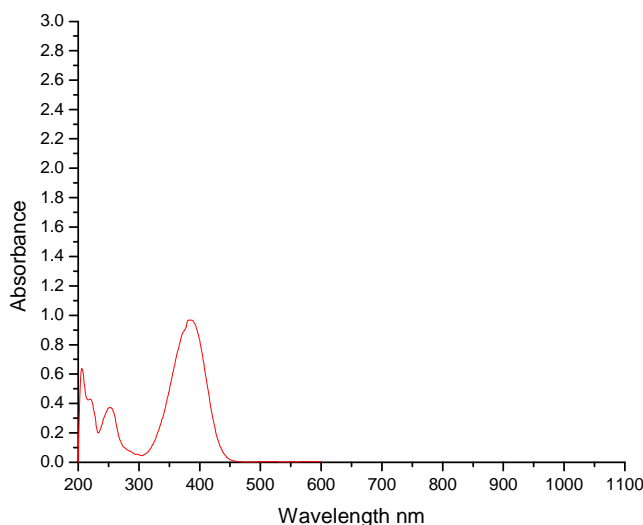
**Fig. 5.** FTIR spectrum of MBST crystal

**Table 2 FTIR Analysis**

Peak $\text{cm}^{-1}$	Assignment
3445.87	OH stretching vibration
3044.23	Aromatic C-H stretch
1588.57	C-C stretch of the olefinic double bond
1513.69 & 1465.52	Aromatic ring skeletal in plane stretching vibration
1341.18 & 1296.24	Asymmetric and symmetric stretching vibrations of $\text{SO}_3$ group
1107.95	Phenolic C-O stretch
837.22	Olefinic C-H bond
668.01	Cis orientation of the substitute at the olefinic double bond

### 3.4 UV- absorption spectrum

The absorption spectrum was recorded on a HITACHI model U-2800 double-beam spectrophotometer in the wavelength range 200–1000 nm in solution form using methanol as solvent. The absorbance is not registered due to its excellent optical behavior until the wavelength of 450 nm (Fig. 6). Absence of absorption in the region between 400 and 1100 nm is an advantage as it is the key requirement for materials having NLO properties [15]. The spectrum gives two peaks, one intense peak at 385 nm corresponding to  $\pi - \pi^*$  transition and another at 250 nm corresponds to  $n - \pi^*$  transition. Two optical band gaps were calculated for these transitions. The band gap corresponds to  $\pi - \pi^*$  is 8.323 eV and for  $n - \pi^*$  is 12.632 eV.

**Fig. 6. UV absorption spectrum of MBST crystal**

### 3.5 Etching studies

The chemical etching is an important tool for the identification of the defects present in the crystals, which enables to develop some of the features such as growth hillocks, etch pits and grain boundaries on the crystal surface. All the surfaces of the MBST crystal were etched in different solvents but methanol was found as the perfect etchant. The etch pit pattern on (0 1 0)

surface of single crystals after etching in methanol for 10 s was recorded as shown in Fig. 7. From the figure it is clear that the crystal has very less defects.



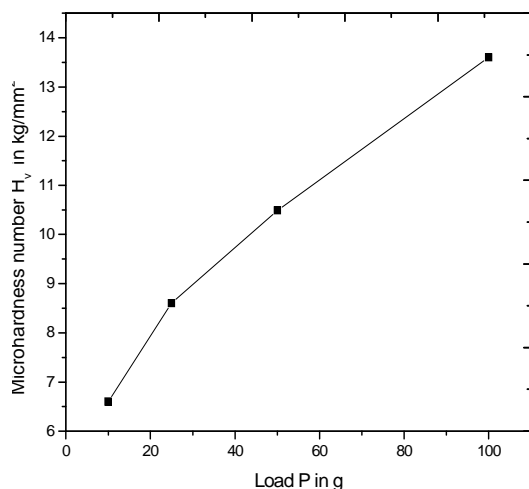
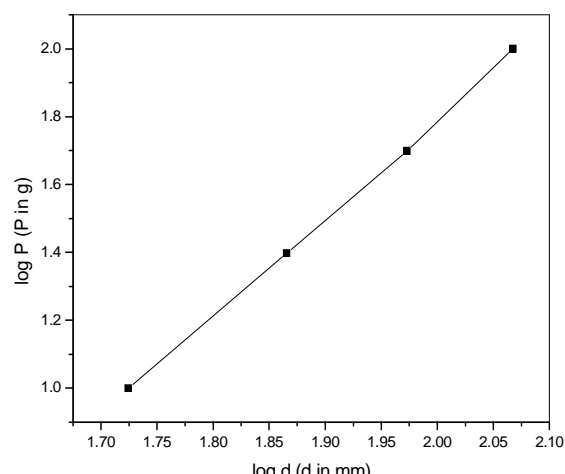
**Fig. 7 Optical micrograph of etched surface**

### 3.6 SHG Efficiency

The relative SHG efficiency of MBST and urea was measured by using the Kurtz powder technique. The sample was subjected to a Q-switched Nd:YAG laser emitting 1064 nm, 10 ns pulse width. The generated SHG signal at 532 nm was split from the fundamental frequency using an IR separator. A detector was used to detect second harmonic intensity connected to power meter to read the energy input and output. The Kurtz powder SHG measurement shows that peak intensity is 17.2 times more than that of Urea.

### 3.7 Microhardness Studies

Vickers hardness indentations were made on the flat polished face of the crystal at room temperature for loads 10, 25, 50 and 100 g using Vickers hardness tester fitted with Vickers diamond intender and attached to an incident light microscope [16]. Crack initiation and material chipping became significant beyond 100 g of the applied load and hardness test thus could not be carried out further. The lengths of the two diagonals of the indentations were measured and the Vickers hardness number was computed using the formula  $H_v = 1.8544 P/d^2$ , where  $H_v$  is the Vickers hardness number in kg/mm<sup>2</sup>, P is the intender load in kg and d is the diagonal length of the impression in mm. A graph was plotted for hardness versus load (Fig. 8) and log P versus log d (Fig. 9). The plot of log P versus log d yields a straight line, and its slope gives the work hardening coefficient or the Meyers index number ‘n’. The value of n is found to be 2.898 and since the value of n is greater than 2, the hardness of the material is found to increase with the increase of load (Fig. 8) which confirms the prediction of Onitsch [17] and also the reverse indentation size effect [18,19]. From the Meyer’s index number it is clear that the title material belongs to soft material category [16].

**Fig. 8. Variation of hardness with load****Fig. 9. Plot of  $\log P$  Vs  $\log d$** 

## CONCLUSION

The organic nonlinear optical material MBST was synthesized and optically good crystals of size  $12 \times 4 \times 3 \text{ mm}^3$  were grown from solution using methanol as solvent. The synthesized compound was confirmed by single-crystal XRD. The functional groups were confirmed from FTIR and SHG studies were in good agreement with the reported literature. The UV–Vis spectrum showed good transparency in the UV and Vis region. Hard- ness measurement shows that MBST crystal is mechanically stable up to 100 g and the increase of the work hardening is may be due to the dislocation motion. Etching studies on MBST reveals very less defects on the surface of the crystal.

## REFERENCES

- [1]B. J. Coe, J. A. Harris, A. K Clays, G. Olbrechts, *et al. Adv. Func. Mater.*, **2002**, 12, 110.
- [2]G.R. Meredith, In: D.J. Williams (Ed.), Nonlinear Optical properties of organic and polymeric materials, (ACS Symposium series 233, American Chemical Society, Washington, DC **1983**) 27.
- [3]Y. Hiroaki Adachi, Takahashi, Junko Yabuzaki, Yusuke Mori, *et al. J. Cryst. Growth*, **1999**, 198/199, 568.
- [4]S.R. Marder, J.W. Perry, W.P. Schaefer, *Science*, **1989**, 245, 626.
- [5]N. Rai, C.W. Lan, *J. Mater. Res.*, **2002**, 17, 1587.
- [6]C.K. Lakshmana Perumal, A. Arulchakkavarthi, N.P. Rajesh, *et al*, *J. Cryst. Growth*, **2002**, 240, 212.
- [7]Stoe and Cie. (**2009**). X-Area V1.52 & X-RED32 V1.48 Software. Stoe & Cie GmbH, Darmstadt, Germany.
- [8]G. M. Sheldrick, *Acta Cryst. A*, **2008**, 64, 112.
- [9]Krishan Lal, G. Bhagavannarayana, *J. Appl. Cryst.*, **1989**, 22, 209.
- [10]G. Bhagavannarayana, S. K. Kushwaha, *J. Appl. Cryst.*, **2010**, 43, 154.
- [11]G. Bhagavannarayana, S. Parthiban, Subbiah Meenakshisundaram, *J. Appl. Cryst.*, **2006**, 39, 784.

- [12]B.W. Batterman, H. Cole, *Rev. Mod. Phys.*, **1964**, 36, 681.
- [13]G. Bhagavannarayana, S. Parthiban, and Subbiah Meenakshisundaram, *Cryst. Growth Des.*, **2008**, 8, 446.
- [14]Krishan Lal and G. Bhagavannarayana, *J. Appl. Cryst.*, **1989**, 22, 209.
- [15]X.M. Duan, S. Okada, H. Oikawa, H. Matsuda, H. Nakanishi, *Jpn. J.Appl. Phys.*, **1994**, 33, 1559.
- [16]S.Kalainathan, K. Jagannathan, *J. Cryst. Growth*, **2008**, 310, 2043.
- [17]E. M. Onitsch, *Mikroskopie*. **1950**, 95, 12.
- [18]K. Sangwal, *Mater. Chem. Phys.* **2000**, 63, 145.
- [19]P. V. Raja Shekar, D. Nagaraju, V. Ganesh, K. Kishan rao, *Cryst. Res. Technol.* **2009**, 44,652.